MAGNETIC RESONANCE IMAGING OF THE LUMBAR SPINE

*NICOLETA CAZACU**,**#, CLAUDIA G. CHILOM***

https://www.doi.org/10.59277/RJB.2024.3.02

*Smeeni Chronic Disease Hospital, Buzău, Romania
**Department of Electricity, Solid Physics and Biophysics, Faculty of Physics,
University of Bucharest, Măgurele, România, Postal address: 405, Atomiștilor St., CP MG - 11,
București-Măgurele, RO - 077125, Romania, #e-mail: nicoleta.sandu@drd.unibuc.ro

Abstract. The objective of this paper is to present the principle of the magnetic resonance imaging (MRI) and its approach in the medical clinic. A comprehensive understanding of the factors contributing to the acquisition of high resolution and contrast images in MRI requires an in-depth analysis of the underlying principles and technical aspects involved. MRI has attracted a great interest in the field of medicine because it does not use harmful ionizing radiation to obtain images of the body, tissues, and organs. In this study, we will find out how MRI is useful in diagnostic of different lumbar spine pathology.

Key words: MRI, basic physical principles, sequences, lumbar spine.

PRINCIPLES OF MRI FOR MEDICAL DIAGNOSIS

Magnetic resonance imaging (MRI) is based on the existence of water molecules in the human body which make up approximately 60–70 % of its composition. For this reason, the most abundant atoms in the body are hydrogens, found in water, but also in fats [9]. The abundance of protons (i.e., hydrogen nuclei) in the human body and its high magnetic moment, and also its high mobility makes it adequate for clinical MRI. Although other nuclei such as carbon, nitrogen, and oxygen can also be used, the protons are the most frequently used for clinical MRI**.**

The protons rotate around an axis and produce their own magnetic field, which will be oriented along the direction of an external magnetic field [32]. Due to their rotation and magnetization, the protons behave as a small permanent magnet. The rotational motion of all charged protons creates a magnetic field or magnetization of the body. This total magnetization can be represented by the magnetic moment

Received: June 2024;
in final form July 2024.

vector. The direction of the magnetization vector is along depending on the strength and direction of the external applied magnetic field (Fig. 1).

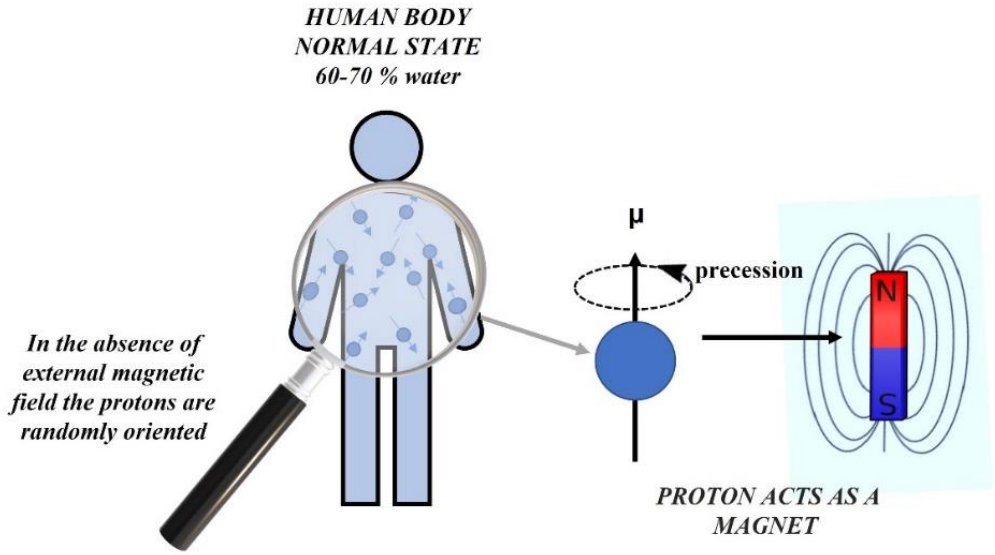

Fig. 1. Randomly oriented proton magnetic moments in the patient body. When the patient is placed inside the MRI scanner, the proton magnetic moments are aligned according to the direction of the external magnetic field. Adapted from Fordham *et al*., 2021 [12], Creative Commons Attribution CC BY license.

Before a patient is placed in an external magnetic field (B_0), the magnetic moments of its protons are randomly oriented (Fig. 1). But, in a strong static external magnetic field (Fig. 2), the magnetic moments of the protons align parallel to it (low-energy nuclei known as *spin-up* nuclei) while a smaller number of the nuclei align anti-parallel (high-energy nuclei known as *spin-down* nuclei) (Fig. 3) [13].

Observation: There are more proton magnetic moments parallel oriented to the external magnetic field at a lower energy level. However, this variation is small and dependent on the strength of the applied magnetic field.

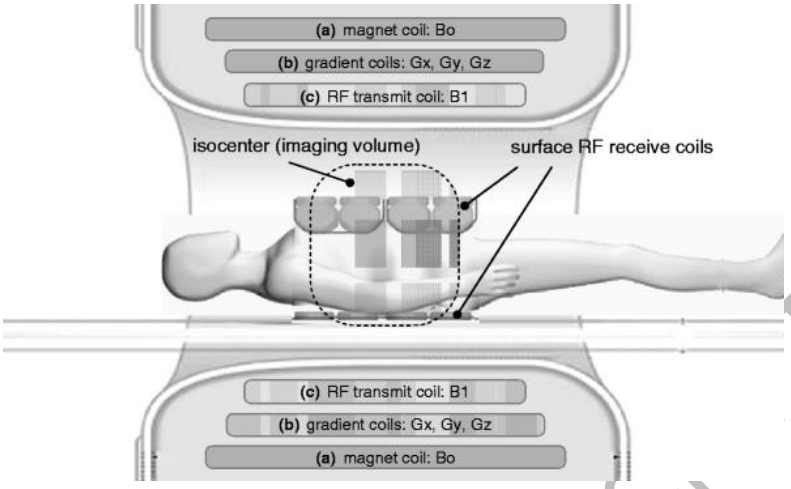

Fig. 2. Scheme of MRI system. (a) magnet coil used to produce the homogeneous static magnetic field (B_0) for spin alignment; (b) gradient coils used to produce the time-varying gradient fields (G_x, G_y and G_z) for spatial encoding of the MR signals, and (c) transmitter radiofrequency (RF) coil to generate a RF field (B_1) for spin excitation [23]. By Moser *et al*., 2009, distributed under the terms of the Creative Commons Attribution CC-BY-NC license.

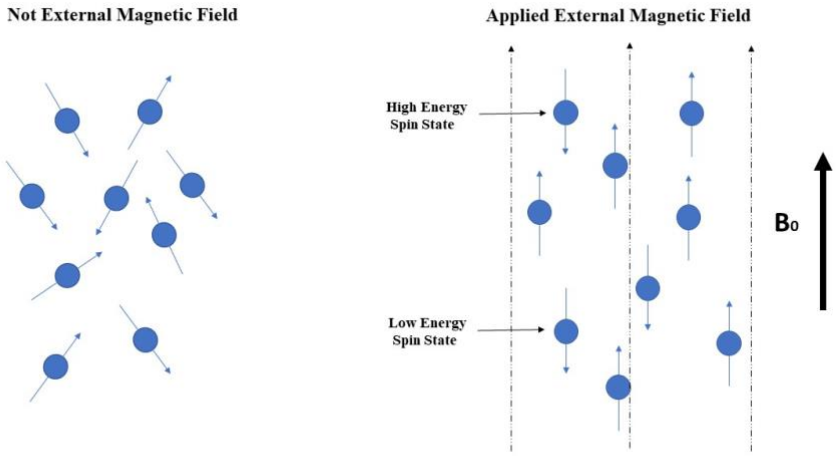

Fig. 3. (Left) In the absence of external magnetic field the protons are randomly oriented. (Right) When the external magnetic field B_0 is applied, it causes the protons to align parallel (in the great majority) or anti-parallel.

After the protons are aligned parallel or antiparallel to the magnetic field, they do not stand in line, but each proton magnetic moment is spinning (i.e., is precessing)

around the axis of the field B_0 [7]. Precession frequency (i.e., Larmor frequency) is not constant and depends upon the strength of the local magnetic field as follows [22]:

$$\omega_0 = \gamma B_{\text{eff}} \quad (1)$$

where: ω_0 is the precession frequency (MHz), γ is the gyromagnetic constant (i.e., the ratio of its magnetic moment to its angular momentum) being different for different nuclei (e.g., ^{1}H = 42.58 MHz/T, ^{13}C = 10.71 MHz/T, ^{19}F = 40.05 MHz/T), and B_{eff} is the local magnetic field strength slightly different from the external magnetic field, B_0 (e.g., 1.5 T, 3 T).

It results from (1) that each active nucleus rotates at different frequencies under the same magnetic field. In homonuclear MRI, one can specifically image only protons ignoring the other active nuclei of the body. A longitudinal magnetic field is created by the parallel alignment of the net magnetic moments of the protons, which leads to a net magnetization of the body in the direction of the external magnetic field. Once the patient is placed inside the MRI machine, he has his own magnetic field but because it is longitudinal it cannot be directly measured.

When a radio frequency (RF) pulse of energy is applied at the Larmor frequency of each proton, the nuclei gain energy and resonates.

Resonance causes the longitudinal net magnetization vector to move out of alignment with B_0 field due to low-energy nuclei gaining enough energy to join the high-energy population. This results in the net magnetization vector lying at an angle to B_0, known as the flip angle (the angle of rotation of the magnetization in the rotating reference frame during the application of a RF pulse), which is determined by the amplitude and duration of the RF pulse [22]. Typically, the flip angle is 90 °, but even with other angles, there is always a perpendicular magnetization component due to the vector nature of the net magnetization vector.

After the RF pulse is turned off, the longitudinal net magnetization vector is influenced by B_0 again, and it attempts to realign with it. The protons must lose the energy from the RF pulse by a process known as relaxation. As relaxation occurs, some high-energy nuclei return to the low-energy population and align their magnetic moments in the spin-up direction, causing the net magnetization vector to realign with B_0. This process has two effects: 1) recovery, where magnetization in the longitudinal plane gradually increases, and 2) decay, where magnetization in the transverse plane gradually decreases. The reduction of transverse magnetization causes a decrease in the voltage induced in the receiver coil, resulting in the free induction decay (FID) signal.

The recovery of longitudinal magnetization is due to a process known as T1 recovery. This occurs when the nuclei transfer their energy to the surrounding environment or lattice, a process called spin-lattice relaxation. Liquids have a lengthy T1 because protons find it difficult to release their energy as the small water molecules move too quickly, whereas fat has a brief T1 because the fatty acid ends

have frequencies close to the Larmor frequency, allowing for efficient energy transfer.

T2 decay is the gradual loss of coherent transverse magnetization caused by neighboring nuclei's magnetic fields interacting with each other. This process is also known as spin-spin relaxation. Water molecules have a long T2 relaxation time, making them sensitive to inhomogeneities of the external magnetic field, and vulnerable to inhomogeneities of the local magnetic fields within the tissues.

IMAGE WEIGHTING

In order to approach the image weighting or contrast it is necessary to introduce repetition time (TR, ms) and the echo time (TE, ms) (Fig. 4). The use of RF pulse sequence constitutes the basis of contrast generation in MRI.

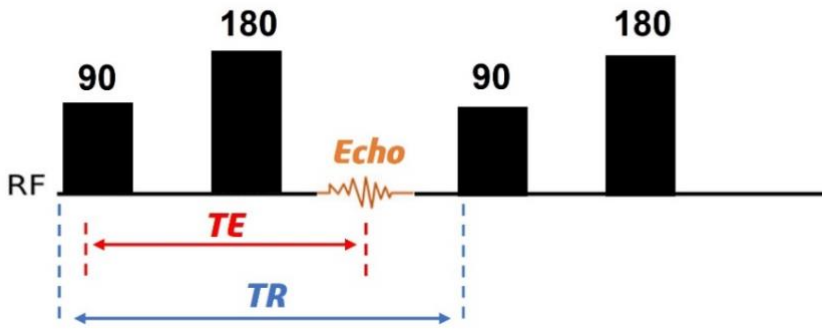

Fig. 4. A basic diagram for TE and TR representation.

TR is the interval between two consecutive 90 ° (or less) RF pulses for each MRI slice. It determines the amount of T1 relaxation that occurs when the signal is read. If a single TR excitation pulse is applied, one can consider TR very long and only T2/T2* contrast can be obtained. T2* is the relaxation time dependent of machine and patient. It describes the decay of the transverse magnetization in the presence of both T2 relaxation and magnetic field inhomogeneities [9].

The reason for using a RF pulse of 90 ° is that it produces the maximum possible signal intensity in the MRI image, while a value less than 90 ° produces a lower signal intensity of the image. Also, using RF pulses with angles greater than 90 ° can produce tissue damage due to excessive energy deposition and tissue heating.

TE represents the time interval from the center of the initial excitation with 90 ° RF pulse and the time when signal reaches the maximum, also known as the echo. It determines the amount of T2 relaxation that has occurred when the signal is read. This parameter is very important because it influences the contrast and resolution of the images.

T1 weighting: The term weighting refers to how the signals from various tissues are adjusted to create a final image. In the case of T1 weighted image, contrast depends on the differences between fat, water and tissues with the intermediate signal. TR is responsible for determining the level of T1 relaxation, which means it determines how much each vector recovers before being stimulated by the next RF pulse.

T2 weighting: The contrast of the T2 weighted image depends on the differences between fat, water, and tissues with the intermediate signal. In this case, the TE setting determines the extent of T2 decay permitted to take place before acquiring the signal. For this situation, TE must be long. If a short TE is used it can be challenging to differentiate between the signals from fat and water, making it difficult for the machine to detect both types of tissue, because both fat and water have similar signal decay rates at short TE values.

MRI PULSE SEQUENCES

The sequences that use a 180 ° pulse to regenerate signal are called spin echo pulse sequences, and those that use a gradient are called gradient echo pulse sequences.

Spin echo (SE) pulse sequences

The spin echo pulse sequence commonly uses two RF pulses, a 90 ° pulse, which rotates the proton magnetic moment with 90 ° away from the magnetic field, and a 180 ° RF pulse, which rotates them by 180 °. The 90 ° pulse initiates the process known as spin echo by tipping the protons 90 ° away from their alignment with the magnetic field, creating transverse magnetization. Then, a 180 ° pulse is applied, which inverts the dephasing spins. As a result, the protons realign with the magnetic field, producing a signal known as the spin echo. This spin echo signal carries valuable information about the tissues and is used to create detailed MRI image. This sequence produces optimum signal-to-noise ratio (SNR) and contrast-to-noise ratio (CNR). The value of magnitude pulse excitation is traditionally used at 90 °.

As one can see in Fig. 5, there are three magnetic field gradients as follow: 1) slice selection (Gss), 2) phase encoding (Gpe) and 3) frequency encoding (Grd). Gradients have important roles in diphase or rephase the magnetic moments of nuclei and in this case in encoding [1,8,10,14,32].

Slice selection gradient is used to locate a specific slice within the selected scan plane. It generates a magnetic field gradient perpendicular to the main magnetic field, allowing for the precise selection of a particular slice within the scanned body.

Phase encoding gradient spatially encodes signal along the short axis of the body anatomy. The phase encoding gradient is applied after slice selection. This gradient varies along the direction perpendicular to the slice plane. It helps in encoding spatial information along this direction. By altering the phase encoding gradient strength during the scanning process, distinct locations within the selected slice can be encoded.

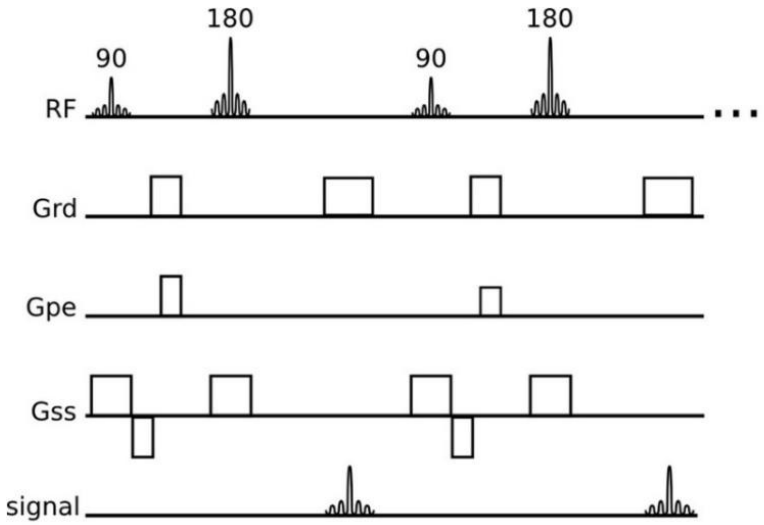

Fig. 5. Spatial encoding in conventional spin echo. RF – radio-frequency pulses, Grd – frequency encoding, Gpe – phase-encode gradient, Gss – slice-selection gradient and signal – acquired echoes [10]. By Ferreira *et al*., 2013 licensee BioMed, distributed under the terms of the Creative Commons Attribution license CC BY (http://creativecommons.org/licenses/by/2.0).

Frequency encoding spatially encoding signal along the long axis of the body anatomy. This gradient varies along the direction parallel to the slice plane. It encodes the frequency information, representing the spatial position along this direction. By altering the frequency encoding gradient strength during the scanning process, various locations within the selected slice can be encoded.

Inversion recovery (IR) sequence is a SE sequence preceded by a 180 ° inverting pulse which is used to selectively null the signal for certain tissues like fat or fluid. The 180 ° inverting pulse reverses the longitudinal magnetization, flipping it to its negative value. The 90 ° readout pulse for the spin echo is then applied after a delay period known as the inversion time (TI). This delay is timed so that the longitudinal magnetization reaches the null point for the tissue we want to suppress [5, 28].

Short Tau Inversion (TI) Recovery (STIR) is an inversion recovery pulse sequence that uses a short TI, also known as tau, (approximately 140 ms at 1.5 T) to suppress the signal from fat [11]. This sequence is widely used in MRI to evaluate edematous changes in the skeleton [21]. In the case of bone tumors or infections one can see a fluid signal in place of normal dark to intermediate marrow signal [16]. The TI used causes fat to recover from full inversion to the transverse plane, such that when the 90 ° RF pulse is applied, there is no longitudinal magnetization corresponding to fat, hence there is no transverse component after excitation and the signal from fat is nulled [32, 16].

Gradient echo (GE) sequences

As in the case of the SE sequences, these sequences also start using a RF excitation pulse, but now the flip angle can be different of 90 ° (usually, smaller), which makes only a part of the longitudinal magnetization to be converted into the transverse magnetization and induce a signal in the receiver coil. When the RF pulse is switched off, due to inhomogeneities in the magnetic field the FID signal is produced and T2* dephasing occurs – a direct result of the fact that there is no 180 ° refocusing pulse for this sequence (Fig. 6) [4]. To obtain T1 and T2 information it is necessary to use a gradient for diphase (removes the phase coherence of the spins) and rephase (removes the dephasing effects, making the spins coherent again) the magnetic moments. As we can see from Fig. 6, in this case is not used a second RF pulse for rephase the transverse magnetization as for SE sequences, but a gradient, named spoiler gradient.

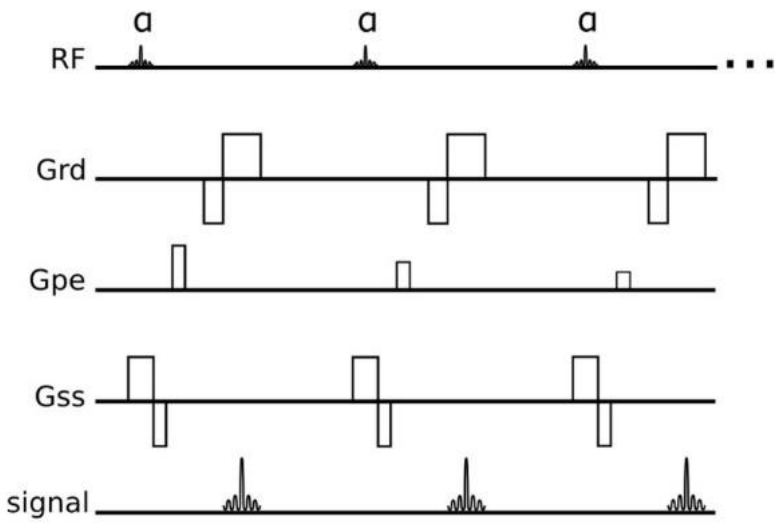

Fig. 6. Conventional gradient-echo pulse sequence. RF – radio-frequency pulses, Grd – frequency encoding, Gpe – phase-encode gradient, Gss – slice-selection gradient and signal – acquired echoes [10]. By Ferreira *et al*., 2013 licensee BioMed, distributed under the terms of the Creative Commons Attribution license CC BY (http://creativecommons.org/licenses/by/2.0).

The signal received by the coil after gradient rephases the magnetic moments with T1 and T2 information is named gradient echo GE) [32]. Usually, GE sequences are used to generate T1 and T2* images. The T2 information obtained from a GE sequence may be influenced by T2* effects and other factors, and it may not represent traditional T2 contrast as in spin echo sequences.

MATERIALS AND METHODS

The protocols used in MRI can vary depending on the patient's clinical condition or diagnosis and they are established together with the radiologist. In this case, a common protocol used in the analysis of the lumbar spine will be presented.

The images and data used in this study were obtained by the authors at the Smeeni Chronic Disease Hospital in Buzău, Romania, using a 1.5 Tesla MRI scanner, Canon Vantage Orian. These materials were collected with appropriate permissions, and written informed consent was obtained from the patients.

For all planes (Sagittal – SAG, Coronal – COR, and Axial – AX), the sequence fast spin echo (FSE) was used. This sequence is faster than the conventional spin echo (SE) technique because after the 90 ° excitation pulse several 180 ° rephasing pulses are used and more than one line of K space is filled per TR [33]. SE also, provides a good conventional image contrast that highlight pathology and is not sensitive to artifacts generated by radiofrequency (RF) and static field inhomogeneity [24]. The use of SE instead of the GE sequence provides some advantages but is important to understand that both sequences have their own specific applications. Among the advantages of applying the SE sequence are: (1) provides better tissue contrast than GE sequences; (2) is less sensitive to B_0 inhomogeneity, GE sequences are more susceptible to artifacts; (3) GE sequences may be sensitive to blood flow, leading to unfavorable signal consequences; (4) simply modified to create various contrasts, such as T1-weighted (T1WI), T2-weighted (T2WI), and proton density [3, 18, 34].

The use of T1WI and T2WI FSE sequences in the investigation of the lumbar spine provides a comprehensive evaluation of the anatomical and pathological structures.

The T1WI FSE sequence provides high-contrast images between tissues with different T1 relaxation times, resulting in high intensity for bones and low intensity for the spinal cord and intervertebral discs. Using this sequence, the detailed anatomy of the lumbar spine and the detection of pathological changes (bone fractures, tumors, bone marrow lesions, vertebral hemangiomas, degenerative disk disease, etc.) can be highlighted [17, 30].

In the case of T2WI FSE are obtained images for tissues with different T2 relaxation times. This sequence provides better visualization for the spinal cord, fluids, and intervertebral discs. Therefore, using this sequence, lesions, osteomyelitis, stenosis, nerve root compression, disc characterization, and other pathology can be better determined [20, 26, 29].

Sagittal T1 inversion recovery (STIR) is used in lumbar spine because it is able to increase the detection of bone marrow diseases [31]. Gupta *et al.*, 2015 [15] showed that using coronal STIR imaging can provide additional diagnose information related to spinal canal stenosis, facet joint arthritis, and ligamentum flavum hypertrophy like sacroiliitis, sacroiliac joint degenerative disease, sacral stress, muscular sprain, and atypical appendicitis.

Table 1 summarizes the parameters utilized for the MRI sequences in this study. These parameters are critical for optimizing image quality and ensuring precise diagnostic outcomes.

Table 1

MRI sequences parameters used for imaging of the lumbar spine

Parameters	SAG T1	SAG T2	COR T2	COR STIR	SAG STIR	AX T2
TR (ms)	585	3970	4614	3450	6035	6257
TE (ms)	10	120	120	120	60	110
TA (min)	02:10	02:52	02:33	04:06	03:50	04:17
Slice thickness (mm)	4.0	4.0	4.0	5.0	4.0	4.0
Interslice gap (mm)	0.8	0.5	0.5	0.5	0.6	0.8
Number of slices	16	16	19	20	17	26
Matrix size	320×320	320×320	288×240	288×288	256×256	256×256
Field of view (mm)	330×330	330×330	330×330	360×360	320×320	200×200

SAG – sagittal plane, COR – coronal plane, AX – axial plane, TA, acquisition time; TE, echo time; TR, repetition time.

The use of different planes is essential because each imaging plane provides different perspectives and advantages, allowing radiologists to evaluate the lumbar spine from multiple angles. Also, using different planes contribute to confirm and accurately characterize various pathologies. Axial images are important for identifying stenosis, disc herniations, and spinal cord abnormalities, while sagittal images are essential for spondylolisthesis, vertebral fractures, and degenerative changes in the intervertebral discs.

RESULTS AND DISSCUSSION

To illustrate the applicability of MRI sequences in imaging lumbar spine pathologies, we will present two case studies and a statistical analysis based on a sample of one hundred patients with lumbar pain.

POST-SURGICAL LUMBAR PAIN A CASE STUDY

Figs 7–9 illustrate the case of a 62-year-old patient who underwent surgical intervention for a herniated disc at the connection, L5-S1 (lumbar 5 and sacral 1), in 2018. The patient has experienced a recurrence of spinal pain, now radiating to the lower extremities.

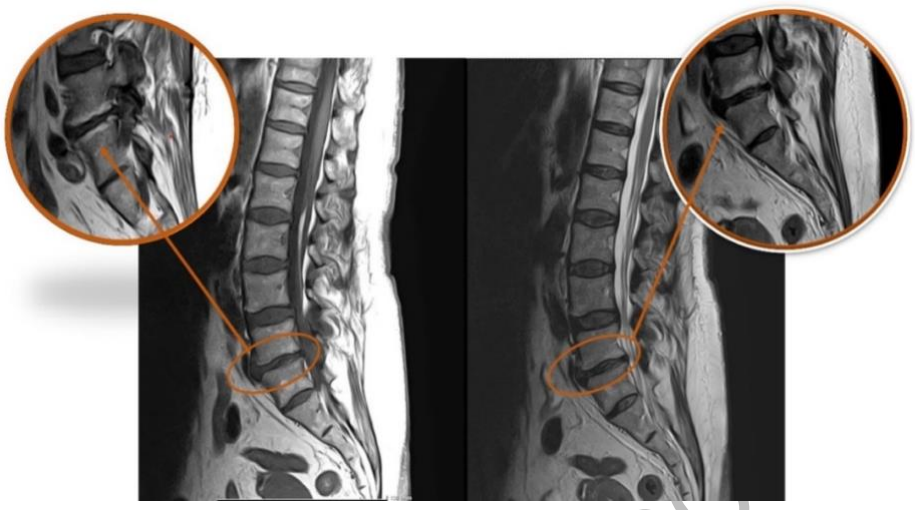

Fig. 7. (Left) T1-weighted sagittal image and (Right) T2-weighted sagittal image. Modic type 2 change – hyperintensity on T1-weighted images and on T2-weighted images at the L5-S1 level.

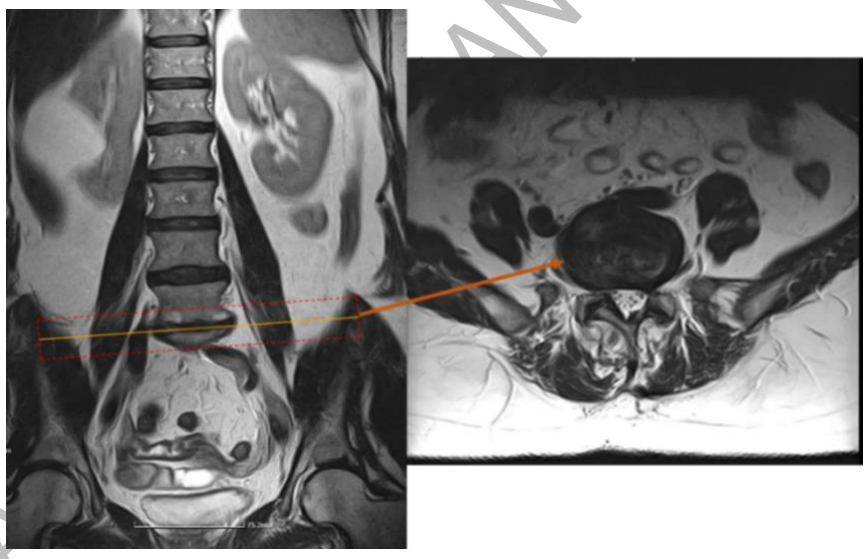

Fig. 8. (Left) T2-weighted coronal image and (Right) T2-weighted axial image. The orange arrows in both the coronal and axial images highlight the specific areas at the L5-S1 level that show post-surgical changes from a left hemilaminectomy.

Following left hemilaminectomy at the L5-S1 level, MRI findings do not indicate signs suggestive of hernia recurrence (Figs 7–9). However, changes in intensity can be observed, affecting the vertebral plateaus adjacent to the L5-S1 intervertebral disc (Figs 7–9). According to the *Modic classification*, which

describes the degenerative changes of the vertebral bodies on MRI, these changes can be characterized as follows: they appear hyperintense on T1-weighted images (Fig. 7, left) and hyperintense on T2-weighted images (Fig. 7, right, Fig. 8, left), indicating a transformation of bone marrow with a high fat content [25]. These findings are consistent with *Modic Type 2* changes, which are associated with fatty replacement of the bone marrow. It can be also seen a hyperintense signal on STIR images (Fig. 9).

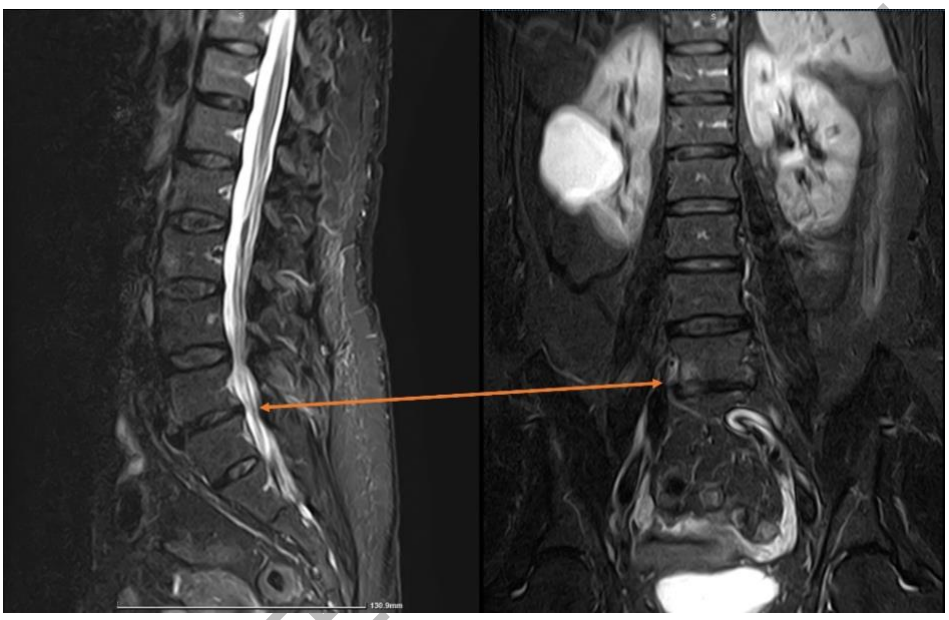

Fig. 9. (Left) STIR sagittal image and (Right) STIR coronal image. At the L5-S1 level, there is high signal intensity within the vertebral body of L5, more prominently visible in the coronal plane than in the sagittal plane.

Additionally, at the L4-L5 level, a small circumferential disc protrusion is noted, small lower lumbar marginal osteophytes and there is also a cyst present in the left kidney (Fig. 8, left and Fig. 9, right). No changes in height or alignment at the level of the lumbar vertebral bodies are present.

MRI-BASED DIAGNOSTIC EVALUATION OF LUMBAR PAIN IN A NON-SURGICALLY TREATED PATIENT

In the following case, is presented a 67-year-old female patient with no history of surgical intervention. She exhibits lumbar pain radiating to the right lower limb, without associated paraesthesia. MRI findings include:

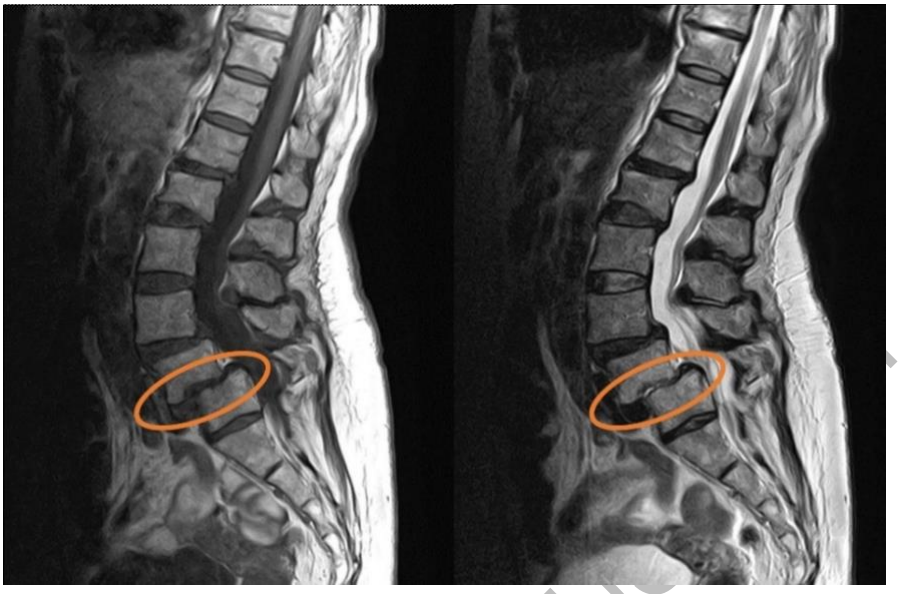

Fig. 10. Sagittal MRI scans of the lumbar spine. (Left) T1-weighted sagittal image and (Right) T2-weighted sagittal image. Accentuation of lumbar lordosis. The orange oval highlights L4 anterior spondylolisthesis.

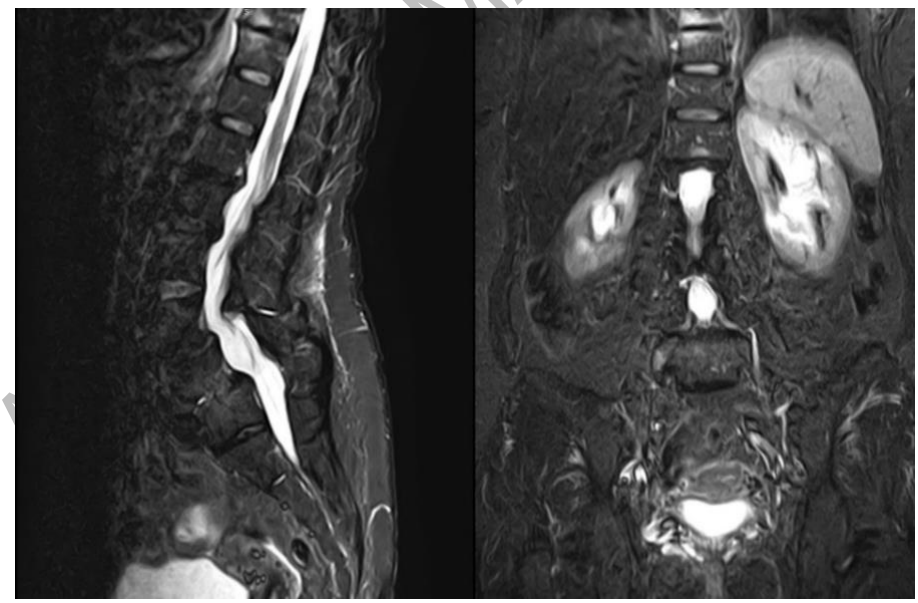

Fig. 11. (Left) STIR sagittal image and (Right) STIR coronal image of the lumbar spine. Coronal plane revealing dextroconvex lumbar scoliosis. Similar degenerative changes as seen in the sagittal plane.

– Lumbar lordosis emphasis on acquisitions in the sagittal plane (Fig. 10 left and right) and dextroconvex lumbar scoliosis visible on acquisitions in the coronal plane (Fig. 11, right). Lumbar vertebral bodies have normal MRI height.

– Anterolisthesis L4 compared to L5 by about 13 mm (Fig. 10 left and right).

– Lumbar circumferential osteophytes.

– Circumferential lumbar disc bulges at the levels of T12-L1, L1-L2, L3-L4, L4-L5, with radicular contact involving the nerve roots of L1, L2, L5 in the bilateral lateral recess, and the nerve roots of L3 and L4 in the bilateral intra-extraforaminal regions (Figs 12–13).

– The lumbar intervertebral discs show obliteration of the differentiation between the annulus fibrosus and the nucleus pulposus, with a grade III appearance according to the *Pfirrmann* classification [27], except for the L4-L5 intervertebral disc, which also has reduced height and a grade IV-V appearance according to the *Pfirrmann* classification.

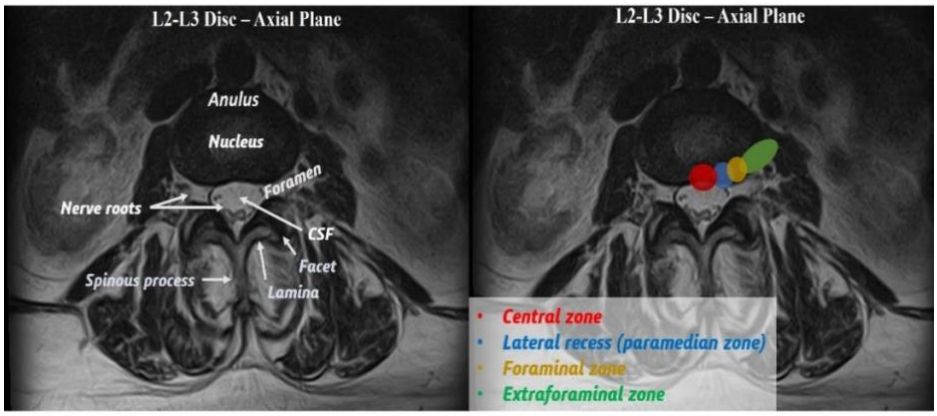

Fig. 12. (Left) Magnetic resonance imaging of L2-L3 disc axial view. (Right) Disc hernia location nomenclature – red: central zone, blue: lateral recess, yellow: foraminal zone, green: extraforaminal zone. The herniation can be combined (e.g., intra/extraformainal, pre/intraforaminal). Adapted from Jeong *et al*., 2024 [19], Creative Commons CC BY-NC license (https://creativecommons.org/licenses/by-nc/4.0).

MRI plays a crucial role in the evaluation of lumbar spine pathologies, providing detailed insights into the structural abnormalities. In this case, MRI helped identify and characterize the extent of degenerative changes, including scoliosis, anterolisthesis, osteophytes, and disc bulges. This comprehensive assessment is essential for guiding appropriate treatment strategies for the patient's lumbar pain and radicular symptoms. MRI parameters are critical in obtaining high-quality images and minimizing artifacts, thereby ensuring accurate patient diagnosis (Table 1).

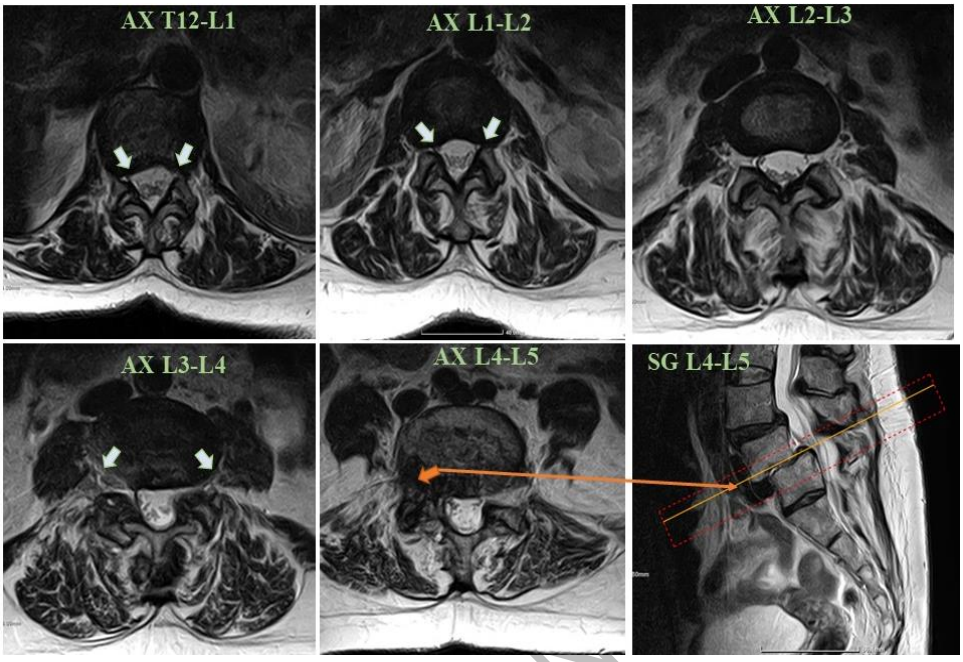

Fig. 13. Magnetic resonance imaging of the lumbar spine. Axial T12-L1 and AX L1-L2 arrows: indicate circumferential disc bulge causing bilateral lateral recess compression; AX L2-L3: no significant disc bulge or nerve root compression noted; AX L3-L4: Indicates circumferential disc bulge causing bilateral intra-extraforaminal nerve root compression at L3. AX L4-L5 arrow indicates circumferential disc bulge causing bilateral intra-extraforaminal nerve root compression at L4 and lateral recess compression at L5. Sagittal L4-L5 red box and orange arrow: show the location and extent of the disc bulge at L4-L5, illustrating its impact on the spinal canal and foramina.

LUMBAR SPINE MRI STATISTICS IN ADULTS WITH BACK PAIN

To better illustrate the importance of MRI in diagnosing lumbar spinal pathology, a statistical study was performed on 100 adult patients with back pain (with or without legs pain) hospitalized in departments of public hospitals who had a MRI of the lumbar spine. MRI-findings were extracted and quantified from radiologists' narrative reports.

As one can see from the schematic illustration (Fig. 14) using the presented sequences (Table 1) it was found that from 100 patients 19.33 % present disk protrusion, 18.91 % static disorders, 14.71 % osteophytes, 13.87 % disk degeneration and disk bulge, 10.5 % disk herniation, 5.46 % hemangioma, and 8 % disk height loss.

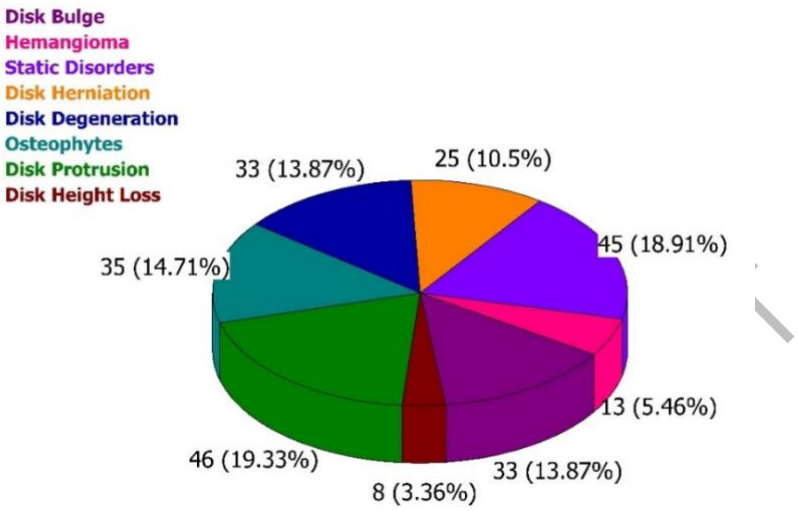

Fig. 14. Pie chart showing proportions of subjects in MR imaging.

The lumbar spine MRI can also be performed using contrast-enhanced which involves the administration of a contrast agent to improve visualization of spinal tumors, infections, vascular abnormalities, and inflammatory conditions. Differentiating between tumor types, determining the degree of tumor involvement, assessing vascularity inside the tumor, and recognizing any related spinal cord compression or nerve root involvement are all made easier by contrast-enhanced magnetic resonance imaging (MRI) [2]. Additionally, it can support therapy response tracking and surgery planning.

Although the primary goal of lumbar spine MRI has traditionally been to acquire precise anatomical imaging, there are efforts to use MRI to assess the functionality of the lumbar region of spine. Functional MRI (fMRI) of the spinal cord is an expanding area of research with potential to investigate neuronal activity in the central nervous system but this may also include the study of the blood flow and tissue metabolism [6]. Challenges include motion artifacts and spatial resolution due to the small size and proximity of the spinal cord to other tissues.

The lumbar spine MRI is one of the most common investigations performed, yet MRI's utility extends far beyond this. Key investigations include brain, cardiac, abdominal, pelvic, and musculoskeletal MRI, covering regions such as the knee, ankle, and shoulder.

CONCLUSIONS

MRI presents a high interest being a non-invasive diagnostic method. In this work only some fundamental and specific physics concepts are presented, in order to help their understanding by MRI operators.

Knowledge of pulse sequences, parameters, and artifacts allows one to identify image distortions, motion artifacts, signal-to-noise ratio issues, and other factors that might affect image clarity and diagnostic accuracy.

MRI of lumbar spine was used as an example because it is one of the most frequent investigated regions.

MRI physics is a fundamental component of image analysis, interpretation, and optimization in lumbar spine imaging ensuring the quality and accuracy of diagnostics.

Funding: This research did not receive any specific grant from funding agencies in the public, commercial, or not-for-profit sectors.

Acknowledgements: The authors are very much indebted to Professor Dr. Aurel Popescu, for very helpful suggestions and permanent encouragement. Additionally, they acknowledge Dr. bioengineer Marilena Gîrban, and the MRI team for their essential support and contributions.

REFERENCES

1. BARRY, C., Gradients: The heart of the MRI machine, *Current Medical Imaging Reviews*, 2006, **2**(1), 131–138.
2. BRADLEY, W.G., Use of contrast in MR imaging of the lumbar spine, *Magn. Reson. Imaging Clin. N. Am.*, 1999, **7**(3), 439–457.
3. BROWN, R.W., Y.C.N. CHENG, E.M. HAACKE, M.R. THOMPSON, R. VENKATESAN, *Magnetic Resonance Imaging: Physical Principles and Sequence Design*, 2nd Edition, Wiley, Hoboken, USA, 2014, ISBN: 978-0471351283.
4. BUXTON, R.B., *Introduction to Functional Magnetic Resonance Imaging Principles and Techniques*, Second Edition, Cambridge, 2009, ISBN-13 978-0-521-89995-6.
5. BYDDER, G.M., J.V. HAJNAL, I.R. YOUNG, MRI: Use of the inversion recovery pulse sequence, *Clinical Radiology*, 1998, **53**, 159–176.
6. COMBES, A., L. NARISETTI, A. SENGUPTA, *et al*., Detection of resting-state functional connectivity in the lumbar spinal cord with 3 T MRI, *Sci. Rep.*, 2023, **13**(18189), 1–11, doi: 10.1038/s41598-023-45302-0.
7. DANCE, D.R., S. CHRISTOFIDES, A.D.A. MAIDMENT, I.D. MCLEAN, K.H. NG, *Diagnostic radiology physics: A handbook for teachers and students*, International Atomic Energy Agency, Vienna, 2014, ISBN 978-92-0-131010-1.
8. DE VOS, B., P. FUCHS, T. O'REILLY, A. WEBB, R. REMIS, Gradient coil design and realization for a halbach-based MRI system, *IEEE Transactions on Magnetics*, 2020, **56**(3), 1–8.
9. ELMAOĞLU, M., A. ÇELIK, *MRI Handbook: MR Physics, Patient Positioning, and Protocols*, 1st Edition, Springer, New York, 2011, ISBN: 1461410959, 9781461410959.
10. FERREIRA, P.F., P.D GATEHOUSE, R.H MOHIADDIN, D.N. FIRMIN, Cardiovascular magnetic resonance artefacts, *J. Cardiovasc. Magn. Reson.*, 2013, **15**(41), 1–39.
11. FISCHER, T., Y.E. BAZ, S. WAELTI, S. WILDERMUTH, S. LESCHKA, S. GÜSEWELL, T.J. DIETRICH, Short tau inversion recovery (STIR) after intravenous contrast agent administration obscures bone marrow edema-like signal on forefoot MRI, *Skeletal Radiol*., 2022, 51(3), 573–579.

12. FORDHAM, A.J., C.C. HACHERL, N. PATEL, K. JONES, B. MYERS, M. ABRAHAM, J. GENDREAU, Differentiating glioblastomas from solitary brain metastases: an update on the current literature of advanced imaging modalities, *Cancers*, 2021, **13**(2960), 1–22, doi: 10.3390/cancers13122960.
13. GROVER, V.P., J.M. TOGNARELLI, M.M. CROSSEY, J.J. COX, S.D. TAYLOR-ROBINSON, M.J. MCPHAIL, Magnetic resonance imaging: principles and techniques: lessons for clinicians, *J. Clin. Exp. Hepatol*., 2015, 5(3), 246–255.
14. GUDINO, N., S. LITTIN, Advancements in gradient system performance for clinical and research MRI, *J. Magn. Reson. Imaging*, 2023, **57**(1), 57–70.
15. GUPTA, R., P. MITTAL, A. MITTAL, K. MITTAL, S. GUPTA, R. KAUR, Additional merit of coronal STIR imaging for MR imaging of lumbar spine, *J. Craniovertebr. Junction Spine*, 2015, **6**(1), 12–15.
16. HAAGA, J.R., D. BOLL, *CT and MRI of the Whole Body*, 6th Edition, 2 volume set, Elsevier, Philadelphia, USA, 2016, ISBN: 978-0323113281.
17. HANRAHAN, C., L. SHAH, MRI of spinal bone marrow: part 2, T1-weighted imaging-based differential diagnosis, *American Journal of Roentgenology*, 2011, **197**(6), 1309–1321.
18. HASHEMI, R.H., W.G. BRADLEY, C.J. LISANTI, *MRI: The Basics*, 3rd Edition, Lippincott Williams & Wilkins, Philadelphia, USA, 2010.
19. JEONG, G., H. PARK, S.J. LEE, D.H. PARK, S.H. PAENG, E. LEE, Imaging of sequestered lumbar discs, *J. Korean Soc. Radiol*,, 2024, **85**(1), 37–23, doi: 10.3348/jksr.2023.0154.
20. KEERTHIVASAN, M.B., B. WINEGAR, J.L. BECKER, A. BILGIN, M.I. ALTBACH, M. SARANATHAN, Clinical utility of a novel ultrafast T2-weighted sequence for spine imaging, *AJNR Am. J. Neuroradiol*., 2018, **39**(8), 1568–1575.
21. KRISTOFFERSEN, P.M., N. VETTI, K. STORHEIM, L.C. BRÅTEN, M.P. ROLFSEN, J. ASSMUS, A. ESPELAND, Short tau inversion recovery MRI of Modic changes: a reliability study, *Acta Radiol. Open*., 2020, **9**(1), 1–10.
22. KUPERMAN, V., *Magnetic Resonance Imaging: Physical Principles and Applications*, 1st Edition, Academic Press, San Diego, USA, 2000, ISBN: 978-0124291508, eBook, ISBN: 9780080535708.
23. MOSER, E., A. STADLBAUER, C. WINDISCHBERGER, H.H. QUICK, M. E. LADD, Magnetic resonance imaging methodology, *European Journal of Nuclear Medicine and Molecular Imaging*, 2009, **36**(1), 30–41.
24. MUGLER 3RD, J.P., Optimized three-dimensional fast-spin-echo MRI, *J. Magn. Reson. Imaging*, 2014, **39**(4), 745–767.
25. NGUYEN, C., S. POIRAUDEAU, F. RANNOU, From Modic 1 vertebral-endplate subchondral bone signal changes detected by MRI to the concept of 'active discopathy', *Annals of the Rheumatic Diseases*, 2015, 74, 1488–1494.
26. PERRY, J., V. HAUGHTON, P.A. ANDERSON, Y. WU, J. FINE, C. MISTRETTA, The value of T2 relaxation times to characterize lumbar intervertebral disks: preliminary results, *AJNR Am. J. Neuroradiol.*, 2006, **27**, 337–342.
27. PFIRRMANN, C.W., A. METZDORF, M. ZANETTI, J. HODLER, N. BOOS, Magnetic resonance classification of lumbar intervertebral disc degeneration, *Spine (Phila Pa 1976*), 2001, **26**(17), 1873–1878, doi: 10.1097/00007632-200109010-00011.
28. SARANATHAN, M., P.W. WORTERS, D.W. RETTMANN, B. WINEGAR, J. BECKER, Physics for clinicians: Fluid-attenuated inversion recovery (FLAIR) and double inversion recovery (DIR) imaging, *International Society for Magnetic Resonance in Medicine*, 2017, **46**(6), 1590–1600.
29. STANKIEWICZ, J.M., M. NEEMA, D.C. ALSOP, B.C. HEALY, A. ARORA, G.J. BUCKLE, T. CHITNIS, C.R. GUTTMANN, D. HACKNEY, R. BAKSHI, Spinal cord lesions and clinical status in multiple sclerosis: a 1.5 T and 3 T MRI study, *J. Neurol. Sci.*, 2009, 279, 99–105.
30. TAMAGAWA, S., D. SAKAI, H. NOJIRI, M. SATO, M. ISHIJIMA, M. WATANABE, Imaging evaluation of intervertebral disc degeneration and painful discs-advances and challenges in quantitative MRI, *Diagnostics*, 2022, **12**(707), 1–16.

31. VAN GOETHEM, J.W.M., Magnetic Resonance Imaging of the Spine, In: P. Reimer, P.M. Parizel, J.F.M. Meaney, F.A. Stichnoth (eds), *Clinical MR Imaging*, Springer, Berlin, Heidelberg, 2010, pp. 197–223.
32. WESTBROOK, C., C.K. ROTH, J. TALBOT, *MRI in Practic*e, 4th Edition, Wiley-Blackwell, Chichester, UK, 2011, ISBN: 978-1-444-33743-3.
33. WESTBROOK, C., *Handbook of MRI Technique*, 3rd Edition, Wiley-Blackwell, Chichester, UK, 2008, ISBN: 978-1-405-18423-6.
34. WESTBROOK, C., *Handbook of MRI Technique*, 4th Edition, Wiley-Blackwell, Chichester, UK, 2014, ISBN: 978-1-118-66162-8.